High-affinity biomolecular interactions are modulated by low-affinity binders

S. Mukundan[1], Girish Deshpande[2*], M.S. Madhusudhan[1#]

[1]Indian Institute of Science Education and Research, Dr. Homi Bhabha road, Pune 411008, India

[2]Department of Molecular Biology, Princeton University, Princeton, NJ, USA

*gdeshpan@princeton.edu

[#]madhusudhan@iiserpune.ac.in

Abstract

Molecular interactions play a central role in all biological processes. The strength of these interactions is often characterized by their dissociation constants (K_D). The high affinity interactions ($K_D \leq 10^{-6}$) are crucial for the proper execution of cellular processes and are thus extensively investigated. Detailed molecular and biochemical analyses of such high affinity interactions have lent considerable support to the concept of binary on/off switches in different biological contexts. However, such studies have typically discounted the presence of low-affinity binders ($K_D > 10^{-3}$) in the cellular environment. In this study, we have assessed the potential influence of these low affinity binders on high affinity interactions. By employing Gillespie stochastic simulations and ordinary differential equations we demonstrate that the presence of low-affinity binders can indeed alter the kinetics and equilibrium of high-affinity interactions. We evaluated the possible impact of such binders in two different contexts including sex determination in *Drosophila melanogaster* and in signaling systems that employ molecular thresholds. Based on these analyses, we speculate that low-affinity binders may be more prevalent in different biological contexts where the outcomes depend critically on threshold value determinants and could impact their homeostatic regulation.

1 Introduction

Key to all biological processes are biomolecular interactions. Networks of these interactions are organised into pathways, that in many instances, intersect (Huh et al., 2003; Kanehisa et al., 2022). These pathways usually consist of tight binding interactions. In a cellular context, these interactions do not occur in isolation but in the presence of a plethora of other molecules and pathways. This in turn ensures that biomolecules can promiscuously interact with multiple partners with varying degrees of affinity.

In this study, we have analysed the influence of low affinity binders on specific high affinity interactions. The strengths of these interactions are reported in terms of their dissociation constants, K_D. Typically, members of a pathway would interact with their partners, with K_D values in the range of 10^{-6} M to 10^{-14} M (Hu, 2017; Perkins et al., 2010), with lower values corresponding to stronger binding. However, the cellular environment consists of a variety of interactors with variable affinities. In addition to its specific high affinity binding partner(s), a biomolecule could encounter a cohort of other binders with K_D values > 10^{-6} M present in the vicinity. These lower affinity interactions are energetically favourable (negative ΔG) as long as the dissociation constant is < 1.

Studies of biological processes usually focus only on the important tight binding interactions resulting in productive outcomes. This is in part because these interactions are canonically considered to be central to cellular processes. Moreover, experimental techniques mostly detect strong interactors (Galaway and Wright, 2020; Jiang and Barclay, 2009; Li et al., 2014). Here, we have examined how the kinetics of these high affinity (tight binding) interactions could be altered and/or modulated in the presence of several low affinity binders. For this study, low affinity interactors were conservatively considered to have K_D values 3 to 6 orders of magnitude less favourable than their stronger counterparts. We also considered the concentration of the low affinity binders to be in the range of 1X to 2X to that of the tight binding partners. This is a conservative estimate as the cellular milieu may contain a higher concentration of the low affinity binding partners, mechanisms for local enrichment of binding partners notwithstanding.

Using these conservative values of binding strengths and relative concentrations, we investigated the effect of weak binding partners on the kinetics and equilibrium of a tight binding interaction. We computed these effects using Gillespie stochastic simulations (Gillespie, 1977, 2013) and ordinary differential equations (ODEs) respectively. We found that the presence of low affinity binders transiently alters the kinetics in a manner that could impact non-equilibrium processes. For instance, consider the following interaction.

$$A + B \rightleftharpoons AB$$

Here, the reactants *A* and *B* interact tightly to form the product *AB*. In the environment are several low affinity binders (A_i and B_i), binding to the two reactants. The rate of formation of *AB* is dependent on the concentration of A_i and B_i. We have studied how the kinetics and equilibrium change with varying levels and binding affinities of A_i and B_i in the cases where – i) there are low affinity binders for either *A* or *B* (B_i and A_i respectively), ii) both reactants have low affinity binders, and iii) there are low affinity binders to *A* and *B* and the A_i's and B_i's are able to interact with each other.

We hypothesize that in a cellular context, such interactions are prevalent as the low affinity binders are likely widespread. Their presence could modulate molecular interactions and hence biological activities. To assess the potential significance of such low affinity binders in a biologically relevant context, we have selected the process of sex determination in *Drosophila melanogaster*. *Sex-lethal* (*Sxl*), a master-switch gene, which determines the

female identity, is turned on by the doubling of X chromosome signal in females. Analysis of mutations in X-chromosome-linked activators has confirmed that activation of early embryonic promoter of *Sxl* (*Sxl-Pe*) is critical in females and thus, underlies the binary fate choice. By contrast, strong repressors capable of affecting sex determination i.e. sex-specific identity and/or viability, have not been identified. Loss of function mutations in such repressors would result in anomalous activation of *Sxl-Pe* in males, which in turn, can induce male to female transformation or lethality. Here, we hypothesise that such repressors are a set of low affinity binders and a single mutation, typically isolated during genetic screens, would not elicit strong phenotypic consequences (e.g. sex-specific lethality) used as stringent criteria for selection. To examine the possible impact of such repressors, we have modelled this system considering *A* as the switch gene, *B* as the X chromosome signal and A_i and B_i as repressors. We demonstrate that our simulation strategy yields outputs that are consistent with previously reported experimental findings. Importantly, our model has also uncovered novel insights into biological processes that depend on molecular thresholds.

2 Results

2.1 The effect of low affinity competitors on the kinetics and equilibrium of strong interactions.

2.1.1 Only one of the strong interactors has competition.

To start with, we examined the effect of low affinity interactors on one of the components of a tight binding complex, i.e., the effect of B_i on the formation of the complex *AB* (see equations E1 and E2). *AB* (dissociation constant $K_D = 10^{-6}$ M) is 5 orders of magnitude stronger than AB_i (dissociation constant $K_{D_i} = 10^{-1}$ M). We have monitored the effect of two parameters, initial levels of the low affinity interactors, B_{i0}, and their binding affinities, K_{D_i}. We simulated the kinetics using the Gillespie stochastic simulation algorithm (Gillespie, 2013) in triplicate and modelled the equilibrium using a system of ordinary differential equations (ODEs). Gillespie stochastic simulations accurately model kinetics for small volume reactions, whereas equilibrium/kinetics estimates derived from ODEs are optimal when reaction volumes are infinite (or very large) (Method section 4.2). Owing to this crucial difference, we selected 500 copies of a molecule in the Gillispie simulations to be 1 mole/litre. This ensured that the trends of the kinetics between the two methods matched, enabling us to compare results from the stochastic simulations and the ODEs. Hence, our units of concentration (moles per litre) does not reflect on physiological concentrations. To be consistent, we have used the same scaling assumption throughout.

First, we studied the effect of B_{i0} levels on the kinetics and equilibrium. The simulation was set up with 500 copies of *A* and *B* and with $K_D = 10^{-6}$ M. Kinetics of reactions with different levels of B_{i0}, ranging from 0 to 1000 were analyzed at $K_{D_i} = 10^{-1}$ M. At the beginning of the reaction the entities *A*, *B* and B_i are present as free monomers. Almost instantaneously, all the monomers of *A* are bound to either *B* or B_i, proportional to their relative abundance. The larger the value of B_{i0}, the longer the system takes to equilibrate (figure 1A). This is because the forward rate constants of the formation of *AB* and AB_i are assumed to be equivalent (for cases where this assumption does not hold see appendix section 8.1). Consequently, the levels of AB_i may be transiently higher than that of *AB*.

AB_i levels decrease while *AB* levels increase since AB_i are more likely to dissociate than *AB.* (Figure 1A). As a result, the average time taken (from 100 replicates) for the formation of *AB* (90% of the maximum possible level) increases linearly with rising levels of B_{i0} (figure 1B). Given the difference in binding affinities, the maximum possible level and the equilibrium value would be numerically similar. The equilibrium concentrations of *AB* and AB_i do not vary with

B_{i0}, even when B_{i0} is 50 times B_0 (figure 1C). This is because the relative affinity of *A* to *B* is 5 orders of magnitude greater than that of *A* to B_i. Thus, the starting level of low affinity interactors influence only the rate of formation of the tight binding complex and has no effect on its equilibrium state.

Separately, we examined the effect of variation in dissociation constant of low affinity interactors on the formation of *AB.* This was done by varying K_{D_i} from 10^1 M to 10^{-9} M while maintaining a B_{i0} level of 500. Decreasing K_{D_i} (increasing the binding strength of the low affinity binder) decreases the rate of formation of *AB* (figure 1D). This decrease is linear in the range of 10^{-3} M to 10^2 M and asymptotic at either end. When K_{D_i} is greater than 10^3 M, the formation of AB complex breaches the 90% level almost instantaneously. At the other extreme, when K_{D_i} is smaller than ~10^{-4} M, the AB complex would reach 90% level at increasingly longer times (tending to infinity) (figure 1E). At equilibrium, AB complex levels would saturate at increasingly lower levels (figure 1F). This is reasonable as the binding affinity of the low affinity interactor is approaching that of the tight binder.

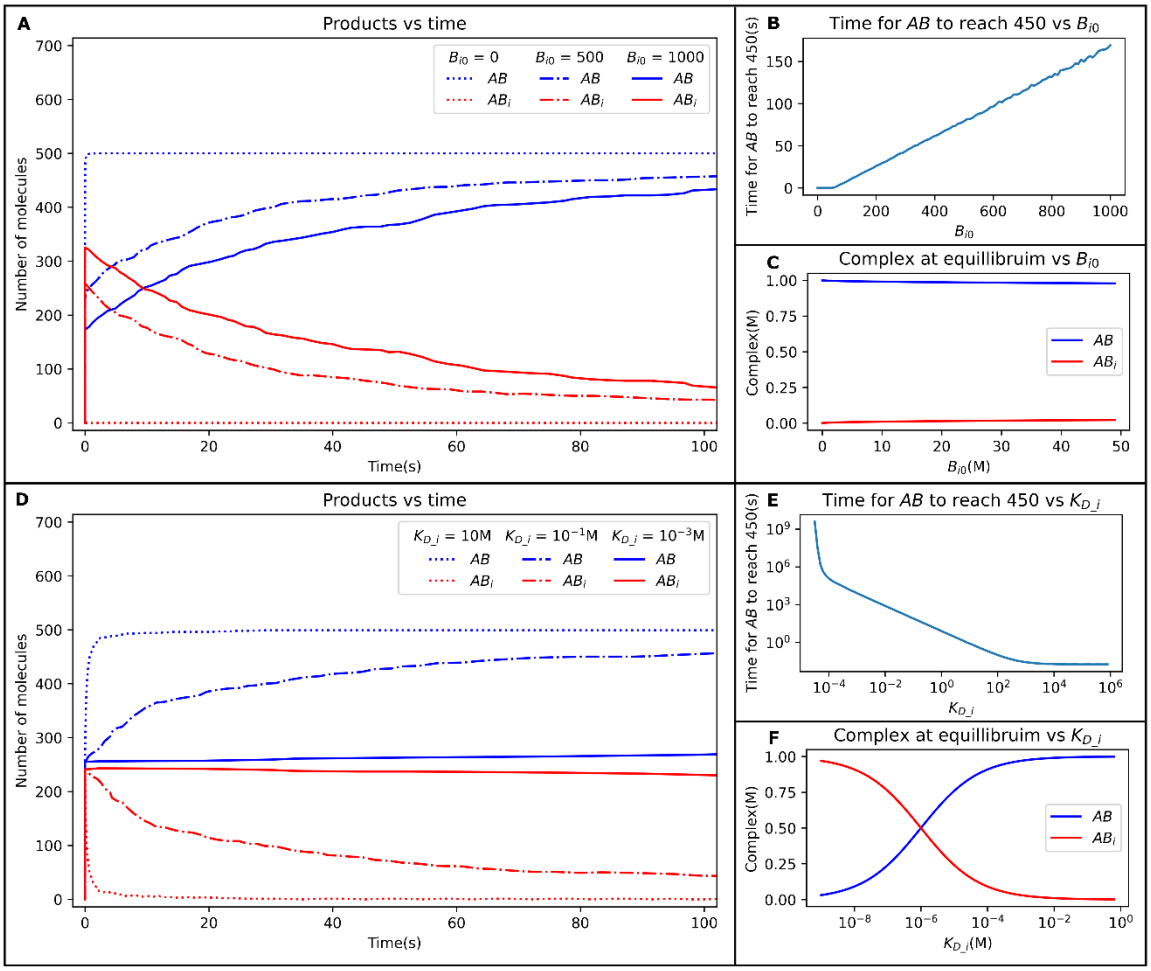

Figure 1: The dependence of complex formation on the starting levels (panels ***A*-C**) and dissociation constants (bottom row panels **D-F**) of the low affinity binder B_i. The kinetics of *AB* (blue lines) and AB_i (red lines) formation at different B_{i0} and K_{D_i} levels (panels **A** and **D** respectively). The time taken for *AB* to reach 450 (90% of the maximum possible value of 500) at different B_{i0} and K_{D_i} levels (panels **B** and **E** respectively). The effect of B_{i0} and K_{D_i} on the *AB* levels at equilibrium (panels **C** and **F** respectively). Panels **A** and **D** show single trajectories taken from triplicate simulations. The lines in panels **B** and **E** are averages over 100 replicates.

The kinetics of these stochastic simulations have been shown deterministically using ODEs (appendix section 8.1). Since low affinity interactors acting on one component of the high affinity interaction can significantly impact the rate of high affinity interaction, we looked at the effect of low affinity interactors on both the high affinity binders in the next section.

2.1.2 Both strong interactors face competition.

In addition to low affinity interactors of A (B_i), we also considered the presence of interactors of B (A_i) in the reaction. A_i interacts with B and forms the complex A_iB (see equations E1, E2 and E3). The dissociation constants of AB_i and A_iB are both described by a single term, K_{D_i}, as we consider them to be equivalent. For this reason, all the results only describe/show AB_i, while the equivalent A_iB is not shown. As in the previous section, the binding affinity of the tight binder (K_D) is 5 orders of magnitude stronger than K_{D_i}. We analyzed the effect of varying the starting levels of B_i and A_i, as well as their binding affinities K_{D_i} on AB formation. As in the previous section, we simulated the kinetics of this system with the Gillespie stochastic simulation algorithm and analyzed the equilibrium states using a system of ODEs.

We first examined the effect of starting levels of B_i and A_i on AB formation. Simulations were set up with 500 copies of A and B and with $K_D = 10^{-6}$ M. The Kinetics of reactions with different levels of A_{i0} and B_{i0}, ranging from 0 to 1000 were analyzed at $K_{D_i} = 10^{-1}$ M. We observed that the presence of low affinity binders decreases the rate of formation of AB (figure 2A). The time taken for AB to equilibrate is around a thousand times more than what we noticed when only B_i was present in the system (figures 1A and 2A). Also, the time taken to reach equilibrium (90% of the maximum possible level) increases exponentially with increasing values of A_{i0} and B_{i0} (figure 2B). The proportion of AB_i increases linearly with increasing values of A_{i0} and B_{i0} (figure 2C).

We then investigated the effect of K_{D_i} on AB formation at values ranging from 10^{1} M to 10^{-9} M. Increasing K_{D_i} increases the time taken for AB to equilibrate (figure 2D). Moreover, at $K_{D_i} = 10^{-3}$ M, the reaction seems to prefer the formation of AB_i, the low affinity complex (figure 2D). We also found that the time taken for AB to reach equilibrium increases with decreasing dissociation constant (figure 2E). At K_{D_i} of 10^{-3} M, AB and AB_i are found at equal levels at equilibrium (figure 2F). This indicates that at K_{D_i} of 10^{-3} M, A is predominantly occupied by low affinity binders even though the affinity for AB formation is 3 orders of magnitude stronger with a K_D of 10^{-6} M.

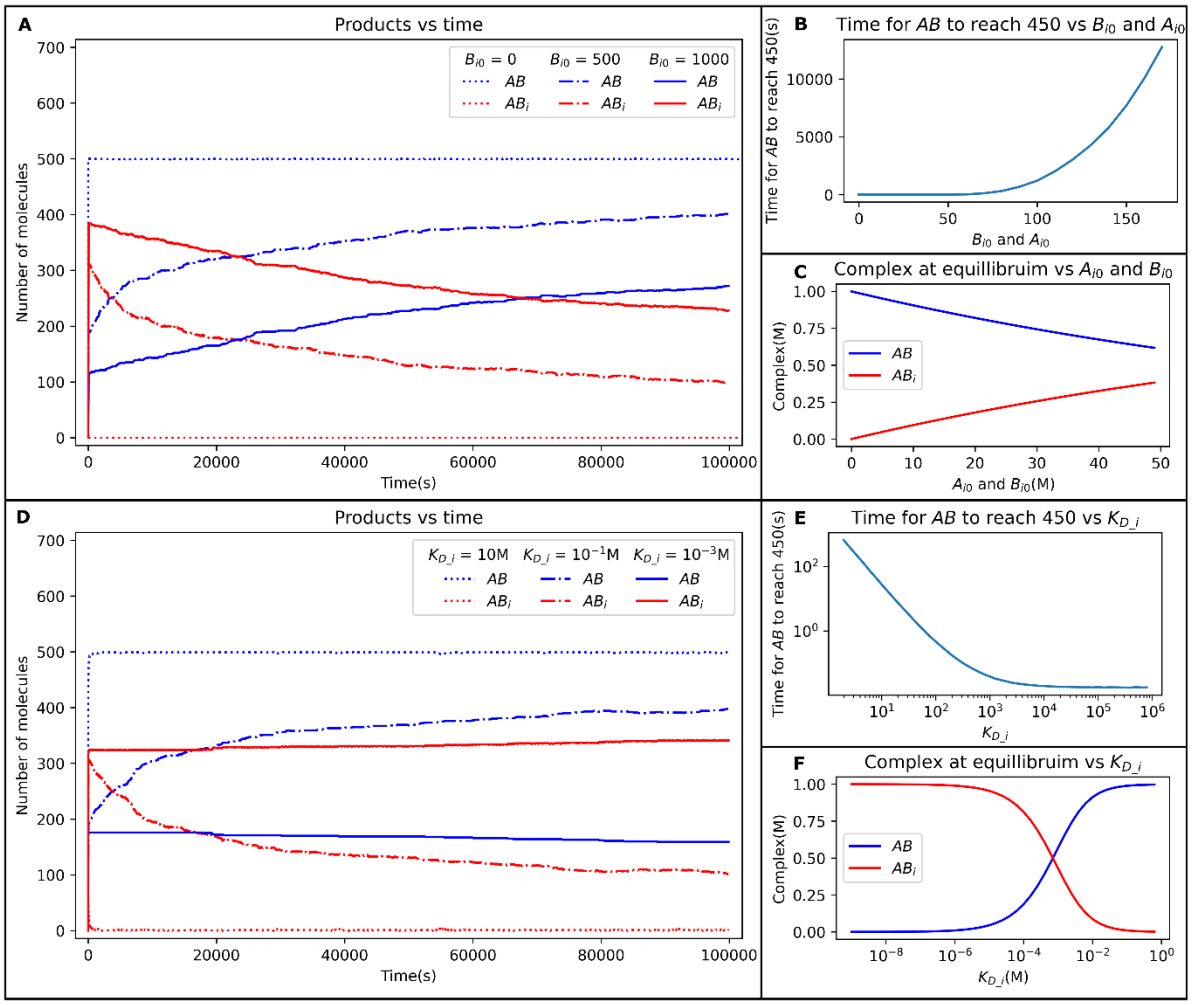

Figure 2: The dependence of complex formation on the starting number (panels ***A***-**C**) and dissociation constant (panels **D**-**F**) of low affinity binders B_i and A_i. The kinetics of *AB* (blue lines) and AB_i (red lines) formation at different starting levels and dissociation constants of B_i and A_i (panels **A** and **D** respectively). The time taken for *AB* to reach 450 (90% of the maximum possible value of 500) at different starting levels and dissociation constants of B_i and A_i (panels **B** and **E** respectively). The effect of different starting levels and dissociation constants of B_i and A_i on the *AB* levels at equilibrium (panels **C** and **F** respectively). Panels **A** and **D** represent single trajectories taken from triplicate simulations. The lines in panels **B** and **E** are averages over 100 replicates.

We have also modelled the kinetics that we observed in this section using ODEs which display a similar trend (Appendix section 8.2). We hypothesize that monomeric A_i and B_i present in the system induce the drastic decline in *AB* formation. This is because monomeric *A* and *B* formed by the dissociation of AB_i or A_iB have a higher chance of interacting with A_i and B_i than another tight binding monomer. To validate this idea, we have analyzed the outcome when free A_i and B_i can interact with one another to produce A_iB_i, a system with minimal amount of monomeric A_i and B_i.

2.2 Interaction amongst the low affinity competitors decrease herd regulation.

We investigated the effect of low affinity interactors A_i and B_i when they can bind to each other to give rise to the reaction product A_iB_i (E4). The dissociation constant of A_iB_i is denoted by K_{D_cross}. We set the dissociation constant for AB_i and A_iB as 10^{-3} M, the strongest example of herd regulation from the previous section (figure 2D). We simulated the effect of cross reaction between A_i and B_i on the kinetics of this system using Gillespie stochastic simulations.

We found that decreasing K_{D_cross} (increasing cross reaction strength) increases the rate of *AB* formation (figure 3A). Also, the time taken for *AB* to reach 90% saturation decreases with decreasing K_{D_cross} (figure 3B). Thus, strong A_iB_i interaction favours active product formation.

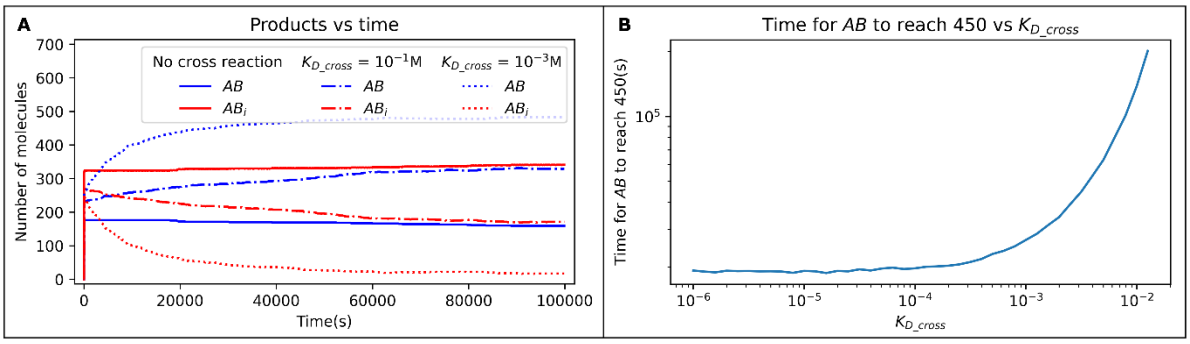

Figure 3: The effect of cross reaction between low affinity inhibitors on herd regulation using Gillespie stochastic simulations. The kinetics of *AB* (blue) and AB_i (Red) complexes at cross-reaction dissociation constants (K_{D_cross}) 10^{-1}M and 10^{-3}M (panel **A**). The effect of K_{D_cross} on the time taken for *AB* to reach 450 (90% of the maximum possible value of 500) (panel **B**). The plot in Panel **B** are averages of 100 replicates. Starting values of *A*, *B* = 500, $K_D = 10^{-6}$M and $K_{D_i} = 10^{-3}$M.

In the last three sections, we have explored the effect of low-affinity interactors on tight binders. In the next two sections, we have examined the effect of herd regulation in deterministic biological contexts and have explored its potential impact on binary outcomes.

2.3 Herd regulation in biological processes.

Here we will illustrate how herd regulation could affect biological processes. In the first case, we will look at sex determination in *Drosophila melanogaster* where a two-fold increase in X chromosome linked signal generates a binary response during the activation of the *Sxl* gene which determines the female identity. The second example is an illustration of biological systems of receptor and ligand that depend on threshold value determinants.

2.3.1 Example 1: Low affinity binders are responsible for the absence of *Sxl* activation in *Drosophila melanogaster* males

Sexual identity in *Drosophila melanogaster* depends on the female specific activation of the binary switch gene Sex-lethal (Sxl) before cellularization at cycle 14 (Cline, 1984). Sxl activation, in turn, is regulated by the Sxl establishment promoter *Sxl-Pe*. This process is dependent on X-linked signal elements (XSEs) and autosomal repressors. As females have two X chromosomes, they are able to produce twice the amount of XSEs as compared to males and can specifically activate *Sxl-Pe*. By contrast, *Sxl-Pe* remains off in males who only have one X chromosome. (In insects, the Y chromosome does not contribute to male determination unlike in mammals). The molecular identities of XSEs are well known (Cline, 1988; Cline and Meyer, 1996; Erickson and Cline, 1993, 1991; Kappes et al., 2011; Keyes et al., 1992; Salz and Erickson, 2010). However, the precise mechanism underlying how the doubling of XSE induces the activation of *Sxl-Pe* remains unknown (Deshpande et al., 1995). Of note, no direct repressor that binds to *Sxl-Pe* during early nuclear cycles has been identified, thus far. Moreover, mutations in deadpan (*dpn*) and groucho (*gro*), two known negative regulators of *Sxl-Pe*, display relatively modest phenotypes (Chen and Courey, 2000; Lu et al., 2008; Mahadeveraju et al., 2020; Paroush et al., 1994; Younger-Shepherd et al., 1992).

Here we test the model that multiple low-affinity binders, capable of interfering with the interaction between activators and *Sxl-Pe*, function as regulators of *Sxl*. As the repression

depends on several low affinity binders, it is relatively straightforward to explain why the forward genetic screens were unable to identify corresponding mutants. Single mutations typically isolated in the genetic screens will not display the requisite phenotype.

Our model posits that sex determination involves one tight binding complex, *AB*, regulated by weaker complexes *ABi* (refer to section 2.1.1, equations E1 and E2). Here, the DNA binding sites in *Sxl-Pe* and XSEs constitute tight binders (*A* and *B*) and form the activating complex (*AB*). Low affinity interactors (B_i) are repressors of *Sxl-Pe* that form the repression complex (AB_i). We assumed that there are 50 binding sites in *Sxl-Pe* (Jinks et al., 2003), 500 XSE activators and 500 repressors. The dissociation constant (K_D) of the active complex is 10^{-6} M which is the lower limit of strong binding. The repression complex has a 1000 fold lower dissociation constant (K_{D_i}) of 10^{-3} M. Here again, we considered identical forward reaction rates, whereas the reverse reaction rates are determined by the dissociation constant. Both XSEs and repressors compete for DNA binding sites in *Sxl-Pe*. We consider *Sxl-Pe* to be engaged in active transcription when 90% (45) of the binding sites are occupied by XSEs.

We used Gillespie stochastic simulations to study the kinetics of this system. We calculated the amount of XSEs and repressor bound to *Sxl-Pe* binding sites after 1000 seconds of simulation time at different starting levels of XSEs and repressors. The simulation time scales are relative to the rate constants and may not correspond numerically to biological times.

We first assessed the activity of *Sxl-Pe* at different starting values of XSEs and repressors. As expected, the promoter is predominantly occupied by the repressors when activator levels are low. Increasing XSE levels elevates the number of activating complexes (figure 4A). Subsequently, we examined the effect of changing repressor levels on *Sxl-Pe* activity. Increasing the starting levels of repressors decreases the number of activator-bound *Sxl-Pe* sites. The binding sites are occupied by an equal number of activators and repressors when starting levels of repressors is twice that of starting levels of XSEs. This is despite a 1000-fold difference in binding affinities (figure 4B).

Next, we focused on the time taken for the activation of *Sxl-Pe,* both in males and females. In wild type *Drosophila melanogaster* embryos, activation of Sxl-Pe results in female fate whereas it remains off in males. Furthermore, this is a time-sensitive process as *Sxl-Pe* is active only between nuclear cycles 11-14 and the sex of the embryo is determined by cellularization. For this, we analyzed the ratio of time taken for *Sxl-Pe* activation in male nuclei and female nuclei in *Drosophila* embryos where sex determination occurs autonomously. The calculations accounted for the fact that the XSE levels in females are twice that in males. We found that this ratio is in a narrow range between 1.8 to 2.4 even when activator levels are varied between 0-1000 (figure 4C). Thus, activation of *Sxl-Pe* in males takes approximately twice as long as compared to females. We arbitrarily selected a test case where the starting level of XSE was 100 (for males) to study the time dependence of sex determination. We analyzed this over a population of 10,000 male and female simulations, each corresponding to a single nucleus. The time distributions in males and females for *Sxl-Pe* activation show two distinct peaks corresponding to the two sexes, with males (on average) taking appreciably more time for activation than females (figure 4D). Note that Sxl activation occurs over a range of time (over thousands of seconds in our simulations). Importantly, this pattern of nearly non-overlapping distributions indicates that within a given time interval, *Sxl-Pe* is activated only in females. There is however a small overlap between the male and female distributions (purple region in figure 4D). This indicates that in a small subset of male nuclei, *Sxl-Pe* is turned on and vice versa in females. If the cellularization event occurs between the two peaks (green dotted line in figure 4D), our model can temporally distinguish male and female *Sxl-Pe* activation. These results were could be reproduced using ODEs (Appendix 8.4). Thus, our simulations suggest that the time constraint imposed upon the activation of *Sxl-Pe* is partially

responsible for its female specific activation. Furthermore, in the absence of such constraints, Sxl-Pe can be active even in male embryos, which has been demonstrated to lead to detrimental consequences (Cline and Meyer, 1996). Altogether our analysis recapitulates both the sex-specificity and the temporal dynamics of *Sxl-Pe* activation.

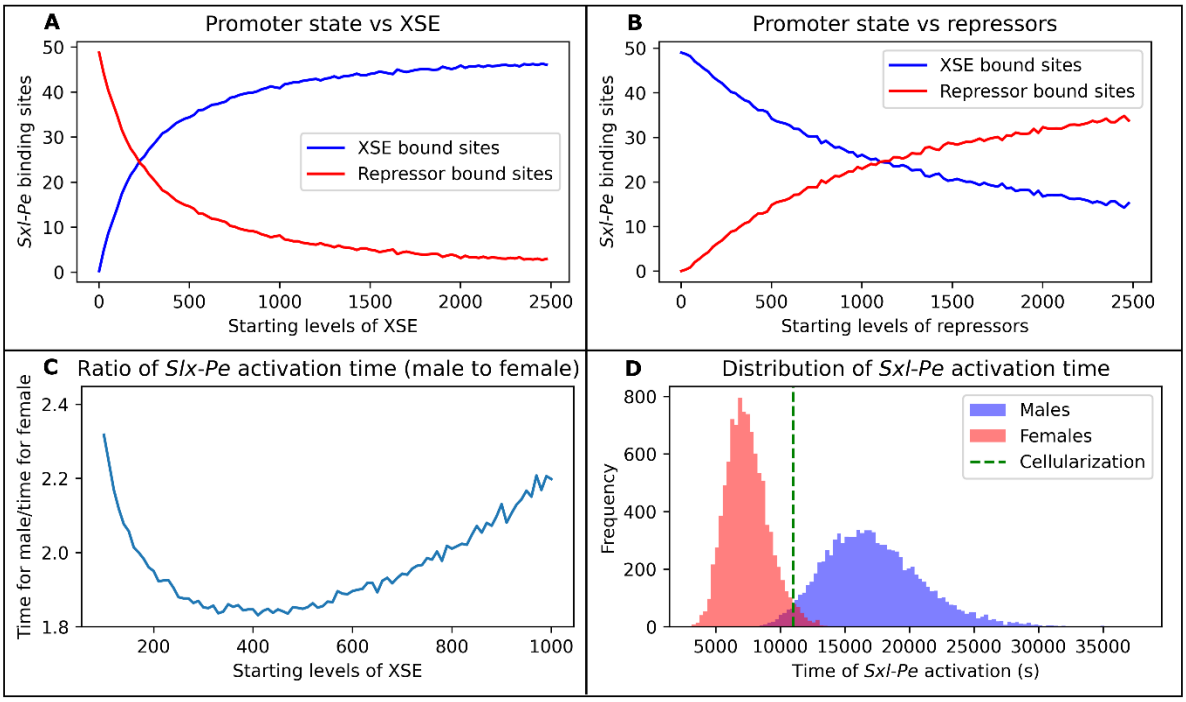

Figure 4: Model of sex determination with one set of low affinity binders. The amount of activating and repressing complexes formed after 1000 seconds at different starting values of XSEs and repressors (Panels **A** and **B**). The ratio of time taken by males vs females to activate *Sxl-Pe* (XSEs occupy 90% of all available *Sxl-Pe* binding sites) (Panel **C**). Panel **D** shows the distribution of time taken for male and female cells to activate across a population of 10000 cells. The simulations were replicated 100 times for each data point in panels **A** and **B**.

2.3.2 Example 2: Signaling thresholds in biological systems can be explained by herd regulation

In general, molecular thresholds are crucial in several biological signaling events ranging from cell fate determination in early development to neuronal action potentials. Without such thresholds, signals resulting from stochastic noise (inherent to crowded cellular environments) would be able to aberrantly activate (or repress) biological processes. In this section, we describe a general molecular mechanism of how herd regulation can be instrumental in establishing such thresholds in biological systems.

Consider the example where receptor *A* is activated by binding a signaling molecule *B* to form the receptor-signal complex *AB*. The system also contains low affinity binders for the receptor and signaling molecule (B_i and A_i respectively) as we have explored in the previous sections. The receptor-signal complex is assumed to have a dissociation complex of 10^{-6} M whereas both the low affinity complexes have a dissociation constant of 10^{-3} M. We modelled the kinetics of this system using the Gillespie stochastic simulation with 50 receptors and 500 signaling molecules. This is in keeping with the observation that signaling molecules are usually in excess compared to the number of receptors (Cima, 1994). The system also contained 500 copies of each of the two low affinity binders. We monitored the levels of the receptor-signal complex (amount of *AB* formed) after 1 million seconds of simulation time,

starting with different levels of the signal (*B*). The time of 1 million seconds was chosen to represent a phase of the reaction that is significantly distant from the fast-starting kinetics. We simulated this system at different starting receptor levels and at levels of the low affinity receptors.

We observed a sigmoidal-like relationship between the number of receptor-signal complexes and the starting levels of the signal. When the number of signaling molecules in the system is below a threshold the rate of increase of the number of receptor-signal complexes is gradual. As soon as the number of signaling molecules exceeds the threshold the number of receptor-signal complexes increases sharply (sigmoid-like). Increasing the levels of the signaling molecule does not alter the threshold but only increases the final levels of the active receptor (figure 5A). Interestingly, we see that the threshold value is regulated by the number of low affinity receptors in the system (figure 5B). Whereas, varying the levels of low affinity signaling molecules does not affect the threshold (figure A8). Thus, the signal threshold is dependent on the level of low affinity receptors in the system, whereas the amplitude of the signal is determined by the number of receptors.

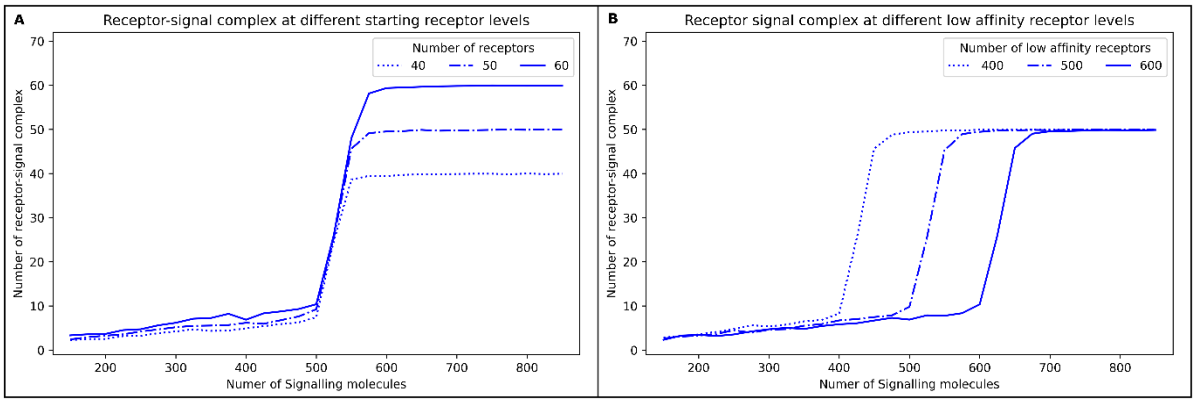

Figure 5: Modeling signaling thresholds in biological systems. All traces (all points are averages of 50 replicates) show the relationship between the active receptor and the number of signal molecules and low affinity complexes at different starting levels of the signal. Panel **A** shows this relation at three different starting receptor levels. Panel **B** shows this relation at different starting levels of the low affinity receptor.

Iyer et al (2022) analyzed the specification of different cell types under the influence of the Wingless morphogen gradient. They proposed that cellular compartmentalization and receptor promiscuity were critical to elicit a specific response to confer unique cell type identities. Interestingly, this was experimentally verified using the modulators of *Wingless* activity, *Dally* and *Dally like* (B_i) which compete with *Frizzled-2* (*B*) receptor for *Wingless* (*A*) binding. The 'Herd regulation' model supports and extends these observations by providing a relatively simple mechanistic explanation for the observed phenomena. We also suggest the presence of undocumented low affinity binders of *Frizzled-2* (A_i). In general, our model could be applied to a number of biological systems where the outcome is contingent upon molecular thresholds.

3 Discussion

Molecular investigations of biological processes almost always focus on interactions that are high affinity and specific. Seldom, if at all, is any importance given to interactions of low affinity/specificity. In part, this could be due to our inability to detect such interactions. In this study, we examine how the presence of low affinity interactors modulates the association of high affinity interactors. We term such modulation of tight binding events by low affinity interactors as 'herd regulation'.

To illustrate herd regulation, we have considered a simple system of 2 interactors (*A* and *B*) that come together to form a dimeric complex (*AB*). We studied the formation of this complex in the presence of low affinity interactors of both *A* and *B*. The first set of computations considered the formation of *AB* in the presence of B_i, a low affinity interactor of *A*. The K_D of AB_i was 10^{-5} times weaker than that of *AB*. Despite this disparity in binding strengths, the presence of low affinity competitors affected the kinetics of the formation of *AB*. In fact, the greater the levels of the low affinity interactor the longer it took for the *AB* complex to form. Finally, at equilibrium, the dominant species is *AB* with nearly no AB_i, regardless of the starting concentrations of B_i.

The kinetics was only further modulated in the background of low affinity interactors to both *A* and *B* (B_i and A_i respectively). In this case, we found that the rate of formation of the *AB* complex increases with changes in the levels of the low affinity interactors. More importantly, *AB* is not the dominant product of the reaction at equilibrium for $K_{D_i} < 10^{-3}$ M, despite K_D of *AB* being 10^{-6}M. At equilibrium, there are equal concentrations of *AB*, AB_i and A_iB. This is in contrast to the previous case and can be explained by the lack of monomeric *A* and *B* in the system, as all available *A* and *B* are consumed by the formation of *AB*, A_iB and AB_i. This is the case since *A* and *B* contribute to the formation of two complexes each, whereas A_i and B_i are a part of only one complex each. Thus, the products of the dissociation of A_iB or AB_i have a higher probability of encountering A_i or B_i compared to *A* or *B*. *AB* is again the dominant product when A_i and B_i can cross react. In this state, there are no monomers present in the system and we see that the effect of herd regulation decreases with the increase in cross reaction strength. Taken together, our results suggest that a herd regulated system can also evolve by mutations that affect the formation of A_iB, AB_i and/or A_iB_i.

In our simple simulations we have demonstrated herd regulation with a binary interaction of *A* and *B* giving *AB* with interference from low affinity competitors A_i and B_i. In the cell, reactions could be more complex, involving multiple reactors with varying stoichiometry. It is thus relatively straightforward to imagine that herd regulation would impact such complex interactions more than it does the simple *AB* system. The other important aspect here is that the low affinity competitors could be multiple species. For instance, the interactor *A* could have many homologous molecules in the cell, all of which could collectively constitute the A_i. Given the sizes and abundances of protein families, our estimates of the levels of the low affinity competitors are conservative.

Unlike our simulations, reactions in the cell do not have all the interactors appearing together at the same instant in time. It is conceivable that before one of the strong binding interactors is introduced into the system, the other binding partner and the low affinity interactors are already present. This would only magnify the effects we have discussed above. i.e., the relative rates of reactions could be slower than what we have simulated, and the time taken to equilibrate the system would be longer. Another factor that could magnify the significance of herd regulation would be the difference in the K_D values between high and low affinity interactors. If the difference were larger than 10^{-5} M, say 10^{-3} M for instance, it would still constitute an undetectable low affinity interaction in many cases, and would only amplify the effects of herd regulation.

In our computations, we have assumed that the forward rate constants ($k_{forward}$ or k_f) for the high and low affinity interactors are the same. This is not an unusual circumstance in biological processes. For instance, proteins that recognize specific sequences of DNA initially bind non-specifically and diffuse along the DNA to its cognate binding site (Kim and Larson, 2007; Shimamoto, 1999; Wang et al., 2006). Non-specifically binding proteins would also have a similar rate of association with the DNA (Cima, 1994). The rates of dissociation, however, are

vastly different and determine the binding affinities. A similar argument can be made regarding protein-protein (or -peptide) and protein-RNA interactions, especially if the binding was predominantly due to complementarity in electrostatics.

We have illustrated herd regulation in biology with two examples. In one, we use protein-protein interactions akin to signal-receptor activation and in another, we use DNA-protein interactions to illustrate sex determination in *Drosophila melanogaster*.

In the example of signaling, we resort to our simple *AB* model (*A* = receptor, *B* = signal or a ligand). The signal (*B*) can bind its cognate receptor *A* or any of the low affinity competitive/homologous receptors A_i. Once *B* is at a level (threshold) where it has saturated all the *A* and A_i's the kinetics is only dependent on the level of B_i (low affinity competing signals). Thus, exhaustion of A_i switches the system, from herd regulation influencing both the tight binders, to one where it affects only a single tight binder. Thus, the threshold is primarily dependent on the amount of A_i, the low affinity receptor, present in the system. This formulation also helps explain earlier observations and computations where the presence of promiscuous receptors (A_i) determine cell fate in *Drosophila melanogaster* development (Iyer et al., 2023).

In the example of sex determination, we analysed a binary switch gene, *Sxl*, whose activity confers female identity. *Sxl* activity is primarily affected by the presence of X-linked signaling elements (XSEs) and autosomal repressors. XSEs are derived from the X chromosome. Thus, females with two X chromosomes activate *Sxl-Pe* while the *Sxl-Pe* of males remains inactive. Sex determination is dependent on the activity of *Sxl-Pe* at the end of the syncytial blastoderm stage of embryogenesis (NC10-13). We have modelled sex determination considering the binding sites in *Sxl-Pe* as *A*, XSEs as *B* and the autosomal repressors as low affinity interactors, B_i. We found that the presence of low affinity binders temporally resolves *Sxl-Pe* activation between males and females. XX and XY genotypes would determine female and male states respectively as long as the cellularization occurs at a time point between male and female activation. The primary factor that allows for this temporal decision is the amount of XSEs, the cell cycle at which cellularization happens and the amount of low affinity autosomal repressors present in the system. Among these, the amount of XSEs and timing of cellularization has been experimentally perturbed. Mutations in XSE genes are detrimental to females (Cline and Meyer, 1996). For instance, delayed cellularization generates embryos with more *Sxl-Pe* activation and vice versa (Erickson and Quintero, 2007). It would be interesting to see the effect of perturbing the low affinity binder levels *in vivo*, although this would require the identification of multiple low affinity binders which would need to be mutated simultaneously. Hypothetically, changing the level of the low affinity repressors (herd regulators) could affect the male-female ratio in a population.

It will be important to consider these data in a broader, more general context. Even a cursory examination should reveal that binary decisions constitute important cornerstones of biological systems both at the 'micro' and 'macro' levels. It is noteworthy that many of the early foundational discoveries, especially in the field of developmental genetics were aimed at uncovering the presence of a single master determinant that functions as a molecular switch. (Sxl is just one such example of the several well documented 'master switch genes'). As the proper execution of the downstream molecular processes is critically dependent on the early choice, these binary switches have proven to be highly effective means to regulate major outcomes of a variety of determinative events. Notwithstanding the benefits however, one ought to consider a few important caveats that are readily overlooked while considering biological relevance and regulation of binary mechanisms that underlie fate determination. The genetic and biochemical strategies aimed at the identification and characterization of

canonical bio-switches (and their regulatory components) invariably rely on phenotypes that are extreme. For instance, the genetic screens that identified regulators of sex determination relied on either male or female specific lethality. (The nomenclature of the relevant mutations *daughterless*, *sisterless a, b* etc. effectively underscores this feature). As the detection of relevant mutations relied on highly penetrant sex-specific lethality, a number of potentially interesting albeit weak mutations were likely dismissed. Their detection is only possible upon simultaneous deletion or addition of multiple weak affinity factors as approximated in our computational approach.

We have also observed an overlap in the distribution of time taken for male and female *Sxl* activation. This suggests that binary switch systems are not strictly binary. Their outcome is actually two states that in many cases can have small (but not insignificant), overlaps. This becomes especially important in the case of cell autonomous determinative events. For instance, the sex of every single cell in a *Drosophila* embryo is independently determined by the total concentration of X-chromosomal elements. As a result, gynandromorphs consist of cells of both sexual identity and, on rare occasions can survive even up to adulthood. While every instance does not result in a dramatic and demonstrable outcome such as this, it is conceivable that several cells of the 'wrong sex' may be determined in an organism and are eventually eliminated (or rendered ineffective) without any detectable consequence. Analogous scenarios can be envisaged in other biological contexts i.e., a few haltere-like cells could co-exist in wings or some neurons may exhibit partial epithelial traits. Such heterogeneity has been well documented in primordial germ cells in blastoderm stage *Drosophila* embryos while its relevance remains to be determined.

Canonical models suggest that both the initiation and maintenance of the binary switch genes follow a stereotypical path toward a unified outcome. Altogether, while binary decisions may lead to invariable and robust outcomes at a macro- or organismal level, cellular heterogeneity likely exists at a micro- or cellular level. Mechanisms ought to be in place that do not allow such variability to exceed permissible limits leading to detrimental biological consequences. Importantly, the tolerable threshold may differ vastly depending on the cellular or organismal contexts. The mechanistic underpinnings and biological relevance of such mechanisms need closer scrutiny and careful consideration as these represent molecular hurdles that are likely essential components of homeostatic mechanisms.

4 Materials and Methods

4.1 Ordinary differential equations to study reaction kinetics and equilibrium.

Consider the following reaction,

$$A + B \rightleftharpoons AB \tag{E1}$$

The rate of change of *AB* is the sum of forward and reverse reaction rates,

$$\frac{d[AB]}{dt} = r_{foward} + r_{reverse}$$

Here, the forward and reverse rates are expressed in terms of concentrations of *A*, *B* and *AB* at a given time, and the rate constants of k_1 and k_{-1} using rate laws.

$$r_{foward} = k_1([A])([B])$$

$$r_{reverse} = -k_{-1}[AB]$$

Thus, the rate of formation of *AB* is,

$$\frac{d[AB]}{dt} = k_1([A])([B]) - k_{-1}[AB]$$

Similarly for the following reactions,

$$A + B_i \rightleftharpoons AB_i \quad \text{(E2)}$$

$$A_i + B \rightleftharpoons A_iB \quad \text{(E3)}$$

$$A_i + B_i \rightleftharpoons A_iB_i \quad \text{(E4)}$$

The rate of formation of each complex can be defined by the following equations.

$$\frac{d[AB_i]}{dt} = k_2([A])([B_i]) - k_{-2}[AB_i]$$

$$\frac{d[A_iB]}{dt} = k_3([A_i])([B]) - k_{-3}[A_iB]$$

$$\frac{d[A_iB_i]}{dt} = k_4([A_i])([B_i]) - k_{-4}[A_iB_i]$$

Since the reactants are shared by the reactions *A*, *B*, A_i and B_i at a given time are affected by multiple reactions and can be expressed as.

$$[A] = [A_0] - ([AB] + [AB_i])$$

$$[B] = [B_0] - ([A_iB] + [AB])$$

$$[A_i] = [A_{i0}] - ([A_iB] + [A_iB_i])$$

$$[B_i] = [B_{i0}] - ([AB_i] + [A_iB_i])$$

The system of differential equations was solved by the fourth-order Runge-Kutta method (dt = 0.001s, except in figure A7 where it is 0.1s) to obtain concentrations and rates of different species over time. A_0 is considered as 0 to study the effect of inhibition on one reaction. K_D for A_iB_i is considered infinity for studying cases without cross reaction.

To compute the state of the reactants and products at equilibrium, ODEs were solved using the sympy module of python assuming the rates of complex formation as 0. Calculations were conducted in jupyter ipython notebooks using python 3, and python 3 scripts (https://github.com/bigbigdumdum/herd_regulation).

4.2 Gillespie stochastic simulations

Differential equations can describe the progression of reactions deterministically. But they assume that the reaction volume is infinitely large, and the stochastic behaviour of molecules is cancelled out. This also means that the concentration terms are continuous. But a cell is a small system with relatively few molecules. In such a system the concentration is no longer continuous, and randomness could often play an important role. We use the Gillespie stochastic simulation algorithm (Gillespie, 2013, 1977) to simulate such a system. This is a numerical method for simulating the temporal evolution of systems of chemical reactions with randomness. It involves iteratively sampling reaction events and updating the state of the system based on the chosen reaction and the current state of the system. And thus can be

used to study the behaviour of complex chemical systems over time, including the effects of noise and uncertainty on the system's dynamics.

We implemented the Gillespie algorithm, in python3 (https://github.com/bigbigdumdum/herd_regulation). First, the initial state of the system is set, including the number and types of reactants and the reaction rates for each chemical reaction. Then, for each possible reaction, the propensity, a measure of the likelihood that the reaction will occur in the next time step, is calculated based on the reaction rate and the current state of the system. *A* random number generator is used to choose one of the possible reaction events based on the propensities calculated. The state of the system is then updated by adding or subtracting reactants as appropriate. The simulation time is advanced by a time step calculated based on the inverse of the maximum propensity and a random number. The process is repeated until the system reaches a) a pre-specified time b) a specified number of iterations or c) when a product crosses a pre-specified level.

5 Acknowledgements

We would like to thank - Dr. Neelesh Soni for help with the Gillespie algorithm, Aditya Marodia for debugging scripts, Dr. Chetan Gadgil for critical reading and criticisms of the manuscript and COSPI lab members for suggestions. The support and the resources provided by 'PARAM Brahma Facility' under the National Supercomputing Mission, Government of India at the Indian Institute of Science Education and Research (IISER) Pune are gratefully acknowledged. SM would like to acknowledge CSIR SRF fellowship. This work was supported by the Department of Biotechnology, Government of India grant to the Indian Institute of Science Education and Research Pune; Department of Biotechnology, India under BICB centre grant (BT/PR40262/BTIS/137/38/2022)

6 Competing interests

None

7 References

Chen G, Courey AJ. 2000. Groucho/TLE family proteins and transcriptional repression. *Gene* **249**:1–16. doi:10.1016/s0378-1119(00)00161-x

Cima LG. 1994. Receptors: Models for binding, trafficking and signaling. By Douglas A. Lauffenburger and Jennifer J. Linderman, Oxford University Press, 1993, $70.00. *AIChE J* **40**:1089. doi:https://doi.org/10.1002/aic.690400624

Cline TW. 1988. Evidence that sisterless-a and sisterless-b are two of several discrete "numerator elements" of the X/A sex determination signal in Drosophila that switch Sxl between two alternative stable expression states. *Genetics* **119**:829–862. doi:10.1093/genetics/119.4.829

Cline TW, Meyer BJ. 1996. Vive la différence: males vs females in flies vs worms. *Annu Rev Genet* **30**:637–702. doi:10.1146/annurev.genet.30.1.637

Deshpande G, Stukey J, Schedl P. 1995. scute (sis-b) Function in Drosophila sex determination. *Mol Cell Biol* **15**:4430–4440. doi:10.1128/MCB.15.8.4430

Erickson JW, Cline TW. 1993. A bZIP protein, sisterless-a, collaborates with bHLH transcription factors early in Drosophila development to determine sex. *Genes Dev* **7**:1688–1702. doi:10.1101/gad.7.9.1688

Erickson JW, Cline TW. 1991. Molecular Nature of the Drosophila Sex Determination Signal and Its Link to Neurogenesis. *Science (80-)* **251**:1071–1074.

doi:10.1126/science.1900130

Erickson JW, Quintero JJ. 2007. Indirect Effects of Ploidy Suggest X Chromosome Dose, Not the X: A Ratio, Signals Sex in Drosophila. *PLOS Biol* **5**:e332.

Galaway F, Wright GJ. 2020. Rapid and sensitive large-scale screening of low affinity extracellular receptor protein interactions by using reaction induced inhibition of Gaussia luciferase. *Sci Rep* **10**:10522. doi:10.1038/s41598-020-67468-7

Gillespie DT. 2013. Gillespie Algorithm for Biochemical Reaction Simulation. *Encycl Comput Neurosci* **1**:1–5. doi:10.1007/978-1-4614-7320-6

Gillespie DT. 1977. Exact stochastic simulation of coupled chemical reactions. *J Phys Chem* **81**:2340–2361. doi:10.1021/j100540a008

Hu W-S. 2017. Kinetics of Biochemical Reactions. *Eng Princ Biotechnol*, Wiley Online Books. doi:https://doi.org/10.1002/9781119159056.ch4

Huh W-K, Falvo J V, Gerke LC, Carroll AS, Howson RW, Weissman JS, O'Shea EK. 2003. Global analysis of protein localization in budding yeast. *Nature* **425**:686–691. doi:10.1038/nature02026

Iyer KS, Prabhakara C, Mayor S, Rao M. 2023. Cellular compartmentalisation and receptor promiscuity as a strategy for accurate and robust inference of position during morphogenesis. *Elife* **12**:e79257. doi:10.7554/eLife.79257

Jiang L, Barclay AN. 2009. New assay to detect low-affinity interactions and characterization of leukocyte receptors for collagen including leukocyte-associated Ig-like receptor-1 (LAIR-1). *Eur J Immunol* **39**:1167–1175. doi:10.1002/eji.200839188

Jinks TM, Calhoun G, Schedl P. 2003. Functional conservation of the Sex-lethal sex determining promoter, Sxl-Pe, in Drosophila virilis. *Dev Genes Evol* **213**:155–165. doi:10.1007/s00427-003-0304-1

Kanehisa M, Furumichi M, Sato Y, Kawashima M, Ishiguro-Watanabe M. 2022. KEGG for taxonomy-based analysis of pathways and genomes. *Nucleic Acids Res* gkac963. doi:10.1093/nar/gkac963

Kappes G, Deshpande G, Mulvey BB, Horabin JI, Schedl P. 2011. The Drosophila Myc gene, diminutive, is a positive regulator of the Sex-lethal establishment promoter, Sxl-Pe. *Proc Natl Acad Sci U S A* **108**:1543–1548. doi:10.1073/pnas.1017006108

Keyes LN, Cline TW, Schedl P. 1992. The primary sex determination signal of Drosophila acts at the level of transcription. *Cell* **68**:933–943. doi:https://doi.org/10.1016/0092-8674(92)90036-C

Kim JH, Larson RG. 2007. Single-molecule analysis of 1D diffusion and transcription elongation of T7 RNA polymerase along individual stretched DNA molecules. *Nucleic Acids Res* **35**:3848–3858. doi:10.1093/nar/gkm332

Li Y-C, Rodewald LW, Hoppmann C, Wong ET, Lebreton S, Safar P, Patek M, Wang L, Wertman KF, Wahl GM. 2014. A Versatile Platform to Analyze Low-Affinity and Transient Protein-Protein Interactions in Living Cells in Real Time. *Cell Rep* **9**:1946–1958. doi:10.1016/j.celrep.2014.10.058

Lu H, Kozhina E, Mahadevaraju S, Yang D, Avila FW, Erickson JW. 2008. Maternal Groucho and bHLH repressors amplify the dose-sensitive X chromosome signal in Drosophila sex determination. *Dev Biol* **323**:248–260. doi:10.1016/j.ydbio.2008.08.012

Mahadeveraju S, Jung Y-H, Erickson JW. 2020. Evidence That Runt Acts as a Counter-Repressor of Groucho During Drosophila melanogaster Primary Sex Determination.

G3 (Bethesda) **10**:2487–2496. doi:10.1534/g3.120.401384

Milo R, Jorgensen P, Moran U, Weber G, Springer M. 2010. BioNumbers--the database of key numbers in molecular and cell biology. *Nucleic Acids Res* **38**:D750-3. doi:10.1093/nar/gkp889

Paroush Z, Finley RLJ, Kidd T, Wainwright SM, Ingham PW, Brent R, Ish-Horowicz D. 1994. Groucho is required for Drosophila neurogenesis, segmentation, and sex determination and interacts directly with hairy-related bHLH proteins. *Cell* **79**:805–815. doi:10.1016/0092-8674(94)90070-1

Perkins JR, Diboun I, Dessailly BH, Lees JG, Orengo C. 2010. Transient Protein-Protein Interactions: Structural, Functional, and Network Properties. *Structure* **18**:1233–1243. doi:https://doi.org/10.1016/j.str.2010.08.007

Salz HK, Erickson JW. 2010. Sex determination in Drosophila: The view from the top. *Fly (Austin)* **4**:60–70. doi:10.4161/fly.4.1.11277

Shimamoto N. 1999. One-dimensional Diffusion of Proteins along DNA: ITS BIOLOGICAL AND CHEMICAL SIGNIFICANCE REVEALED BY SINGLE-MOLECULE MEASUREMENTS *. *J Biol Chem* **274**:15293–15296. doi:10.1074/jbc.274.22.15293

Sims CE, Allbritton NL. 2007. Analysis of single mammalian cells on-chip. *Lab Chip* **7**:423–440. doi:10.1039/b615235j

Wang YM, Austin RH, Cox EC. 2006. Single molecule measurements of repressor protein 1D diffusion on DNA. *Phys Rev Lett* **97**:48302. doi:10.1103/PhysRevLett.97.048302

Younger-Shepherd S, Vaessin H, Bier E, Jan LY, Jan YN. 1992. deadpan, an essential pan-neural gene encoding an HLH protein, acts as a denominator in Drosophila sex determination. *Cell* **70**:911–922. doi:10.1016/0092-8674(92)90242-5

8 Appendix

8.1 Herd regulation of *AB* interaction by low affinity competitor B_i using differential equations

In this section, we have modelled the effect of low affinity binders on one of the tight binders using coupled ODEs (section 4.1, E1, E2). There are infinite forward and reverse rate constants that can be obtained from a dissociation constant. We study three such combinations where: 1) K_D only affects the reverse rate constant, 2) K_D only affects the forward rate constant and 3) both forward and reverse rate constants are equally affected by K_D.

8.1.1 K_D only affect the reverse rate constant ($k_f = 1 \; and \; k_r = K_D$)

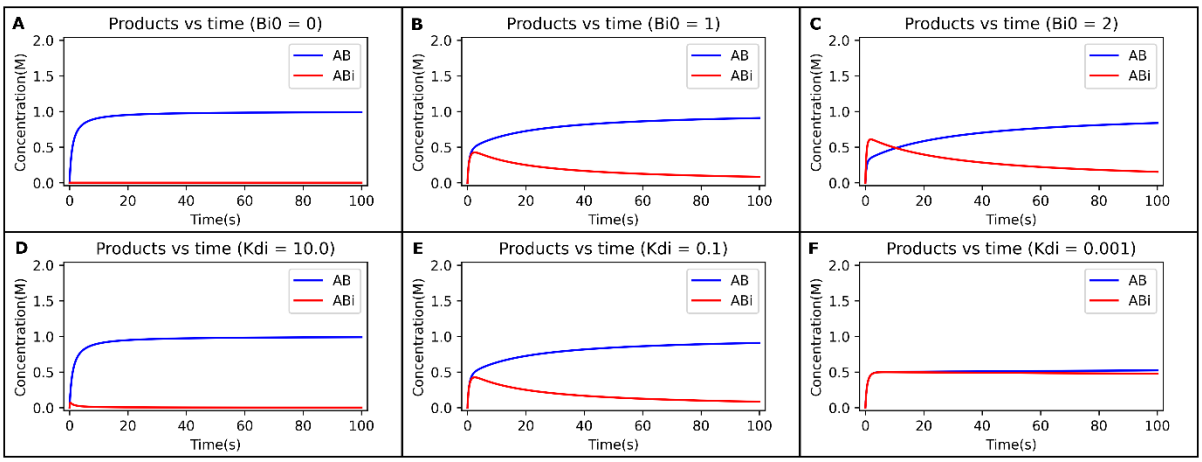

Figure A1: Kinetics while keeping k_f constant. Panels ***A***, ***B*** and **C** show the kinetics of *AB* and AB_i formation at different initial concentrations of B_i. Panels **D**, **E** and **F** show the kinetics of *AB* and AB_i formation at different binding affinities for the inhibitor. Parameters A_0, B_0, B_{i0} = 1M; K_{D_i} = 10^{-1}M and K_D = 10^{-6}M. The values were calculated using Runge-Kutta 4th order integration with time steps of 10^{-6}s.

8.1.2 K_D only affect the forward rate constant ($k_f = \frac{1}{K_D}$ and $k_r = 1$)

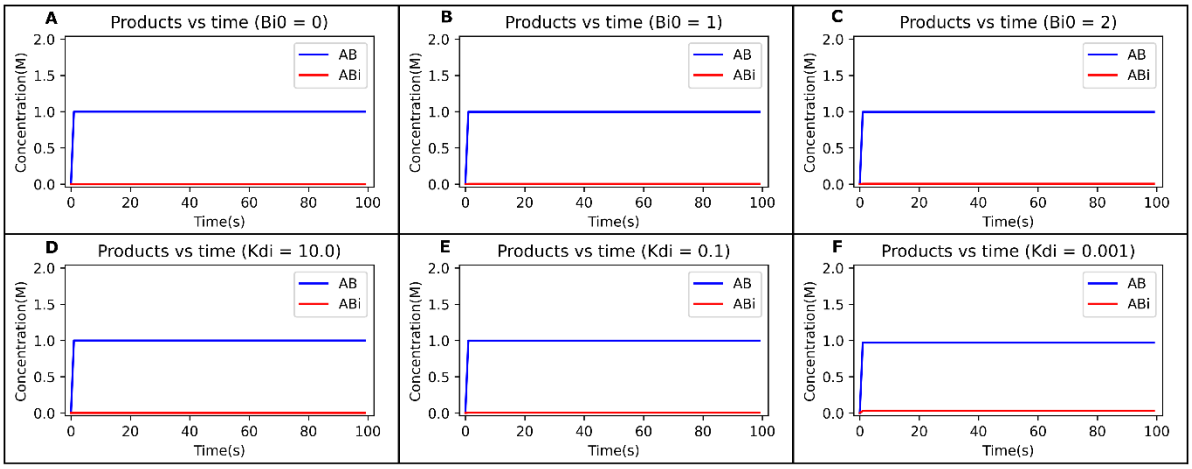

Figure A2: Kinetics while keeping *kr* constant. Panels ***A***, ***B*** and **C** show the kinetics of *AB* and AB_i formation at different initial concentrations B_i. Panels **D**, **E** and **F** show the kinetics of *AB* and AB_i formation at different binding affinities for the inhibitor. Parameters are A_0, B_0, B_{i0} = 1M; K_{D_i} = 10^{-1}M and K_D = 10^{-6}M. The values were calculated using Runge-Kutta 4th order integration with time steps of 10^{-6}s.

8.1.3 Forward and reverse rate constants are affected by K_D equally ($k_f = \frac{1}{K_D^{\frac{1}{2}}}$ and $k_r = K_D^{\frac{1}{2}}$)

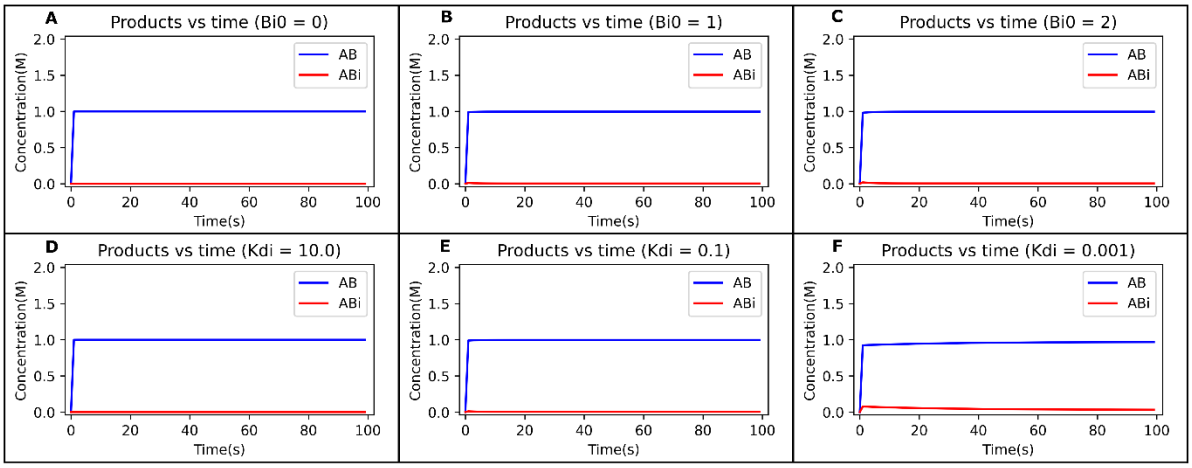

Figure A3: Kinetics when binding affinity is determined equally by forward and reverse reaction. Panels ***A***, ***B*** and **C** show the kinetics of *AB* and AB_i formation at different initial concentrations B_i. Panels **D**, **E** and **F** show the kinetics of *AB* and AB_i formation at different binding affinities for the inhibitor. Default parameters are A_0, B_0, B_{i0} = 1M; K_{D_i} = 10^{-1}M and K_D = 10^{-6}M. The values were calculated using Runge-Kutta 4th order integration with time steps of 10^{-6}s.

When we consider the presence of only one type of low affinity binder, the effect of herd regulation is pronounced only when the forward rate constants are similar.

8.2 Model of herd regulation on both tight binders using differential equations.

In this section, we model the effect of low affinity binders on both tight binders using coupled ODEs (section 4.1, E1, E2, E3). We have modelled the same three cases for interpreting rate constants from the dissociation constant.

8.2.1. K_D only affect the reverse rate constant ($k_f = 1$ *and* $k_r = K_D$)

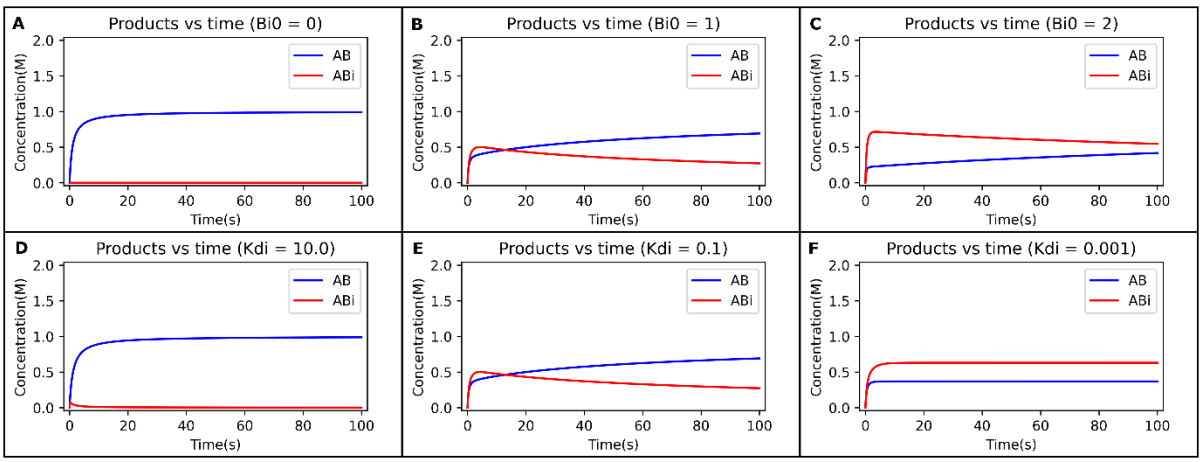

Figure A4: Kinetics while keeping k*f* constant. Panel ***A***, ***B*** and **C** show the kinetics of *AB* and AB_i formation at different initial concentrations B_i. Panels **D**, **E** and **F** show the kinetics of *AB* and AB_i formation at different binding affinities for the inhibitor. Default parameters are A_0, B_0, B_{i0}, A_{i0} = 1M; K_{D_i} = 10^{-1}M and K_D = 10^{-6}M. The values were calculated using Runge-Kutta 4th order integration with time steps of 10^{-6}s.

8.2.2 K_D only affect the forward rate constant ($k_f = \frac{1}{K_D}$ *and* $k_r = 1$)

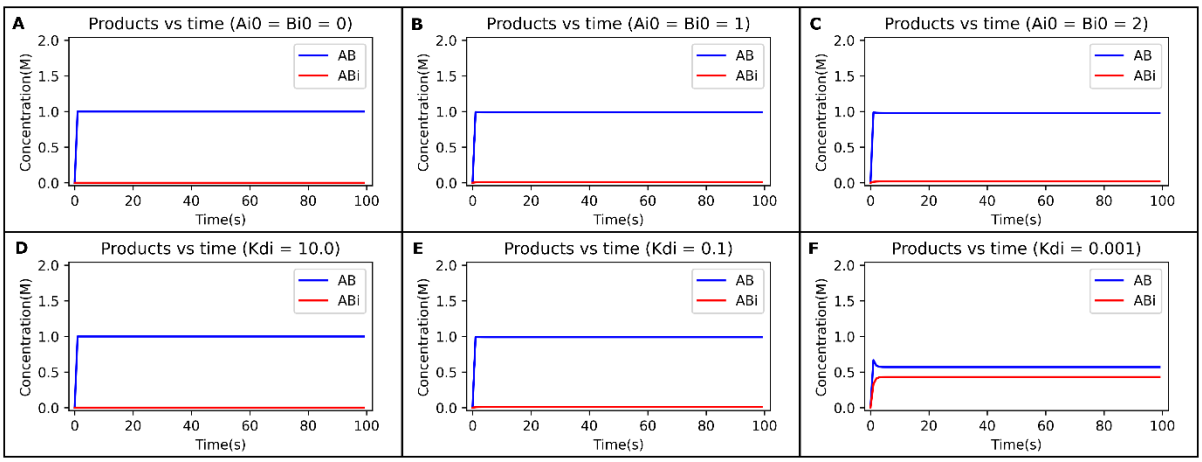

Figure A5: Kinetics while keeping kr constant. Panels ***A***, ***B*** and **C** show the kinetics of *AB* and AB_i. Panels **D**, **E** and **F** show the kinetics of *AB* and AB_i formation at different binding affinities for the inhibitor. Default parameters are A_0, B_0, B_{i0}, A_{i0} = 1M; K_{D_i} = 10^{-1}M and K_D = 10^{-6}M. The values were calculated using Runge-Kutta 4th order integration with time steps of 10^{-6}s.

8.2.3 K_D affects both forward and reverse rate constants ($k_f = \frac{1}{K_D^{\frac{1}{2}}}$ and $k_r = K_D^{\frac{1}{2}}$)

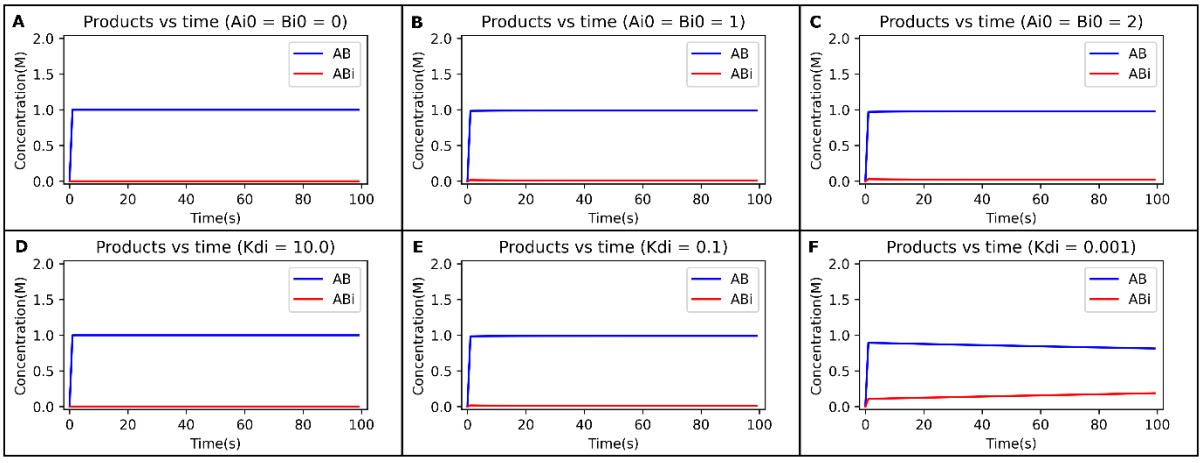

Figure A6: Kinetics when binding affinity is determined equally by forward and reverse reaction. Panel ***A***, ***B*** and **C** show the kinetics of *AB* and AB_i. Panels **D**, **E** and **F** show the kinetics of *AB* and AB_i formation at different binding affinities for the inhibitor. Default parameters are A_0, B_0, B_{i0}, A_{i0} = 1M; K_{D_i} = 10^{-1}M and K_D = 10^{-6}M. The values were calculated using Runge-Kutta 4th order integration with time steps of 10^{-6}s.

8.3 Effect of cross reaction on herd regulation modelled using differential equations

Here the effect of cross reaction is modelled using differential equations.

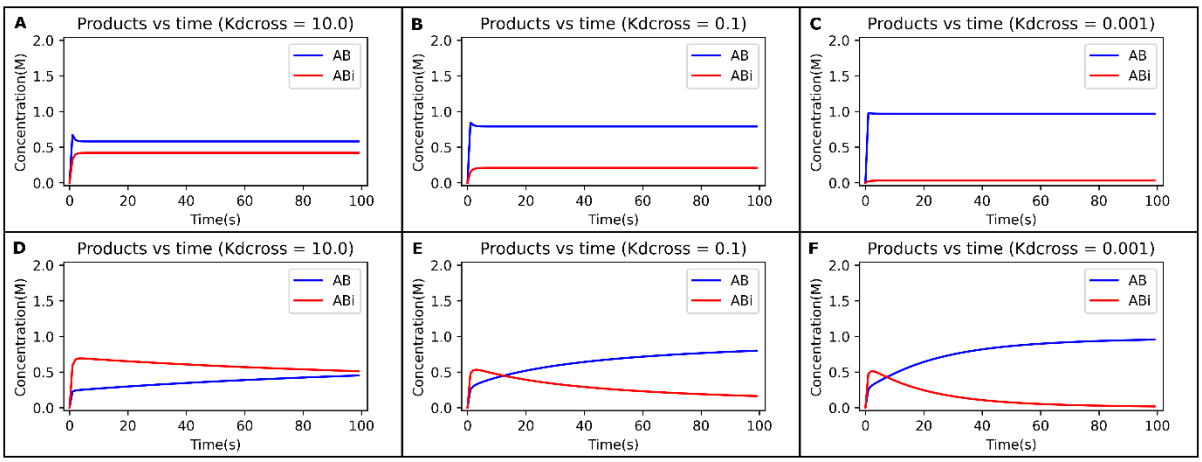

Figure A6: Effect of cross reaction on the kinetics of formation of *AB* and AB_i. Panels ***A***, ***B*** and **C** show the effect of cross reaction of increasing binding affinities on the reaction from figure A4F. Panels **D**, **E** and **F** show the effect of cross reaction of increasing binding affinities on the reaction shown in figure A4C. Parameters used are A_0, B_0, B_{i0}, A_{i0} = 1M; K_{D_i} = 10^{-1}M and K_D = 10^{-6}M. The values were calculated using Runge-Kutta 4th order integration with time steps of 10^{-6}s.

8.4 Sex determination in *Drosophila melanogaster* modelled using differential equations.

Differential equations were used to model sex determination in Drosophila melanogaster. *A* similar approach was used in the study shown under the result section 'Delayed *AB* formation in males can explain differential activation of SXL gene in males and females.' The differential equation results replicate the results obtained with Gillespie simulations.

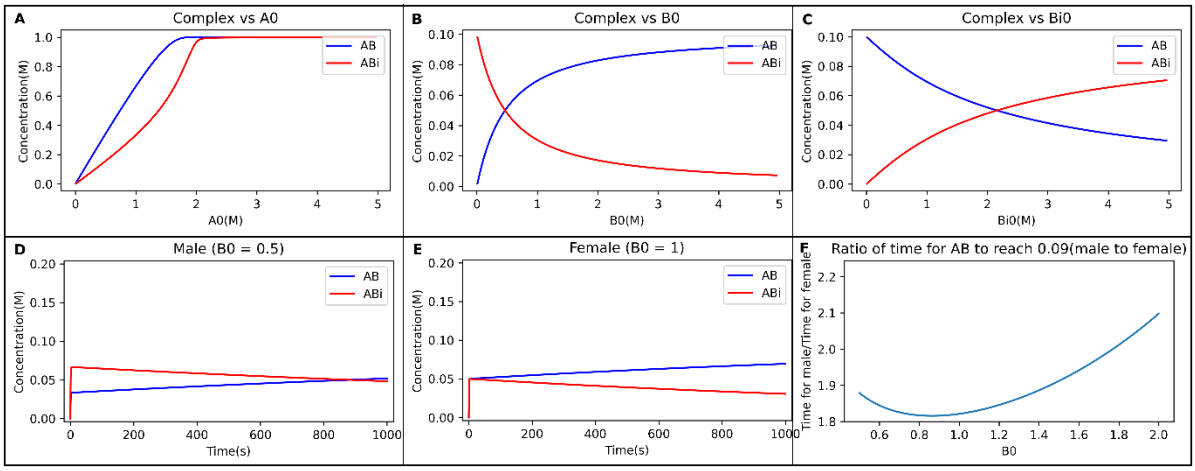

Figure A7: Differential equations were used to replicate the model of sex determination. Panels ***A***, ***B***, and **C** show the concentration of *AB* after 1000 seconds from the start of the reaction, at ranges of different parameters. Panel **F** shows the ratio of time taken by males vs females for *AB* to reach 90% of the value of *A*. This signifies that 90% of the binding sites in *A* are occupied by activators. Panels **D** and **E** are examples of males showing a delayed accumulation of activator complex *AB* compared to females. This example was drawn from panel **F**. Parameters are *A* = 0.1M, *B* = 1M, B_i = 1M, K_D = 10^{-6}M, K_{D_i} = 10^{-3}M and dt (for RK4 integration) is 0.1s.

8.5 Effect of changing levels of low affinity signaling molecules on the threshold.

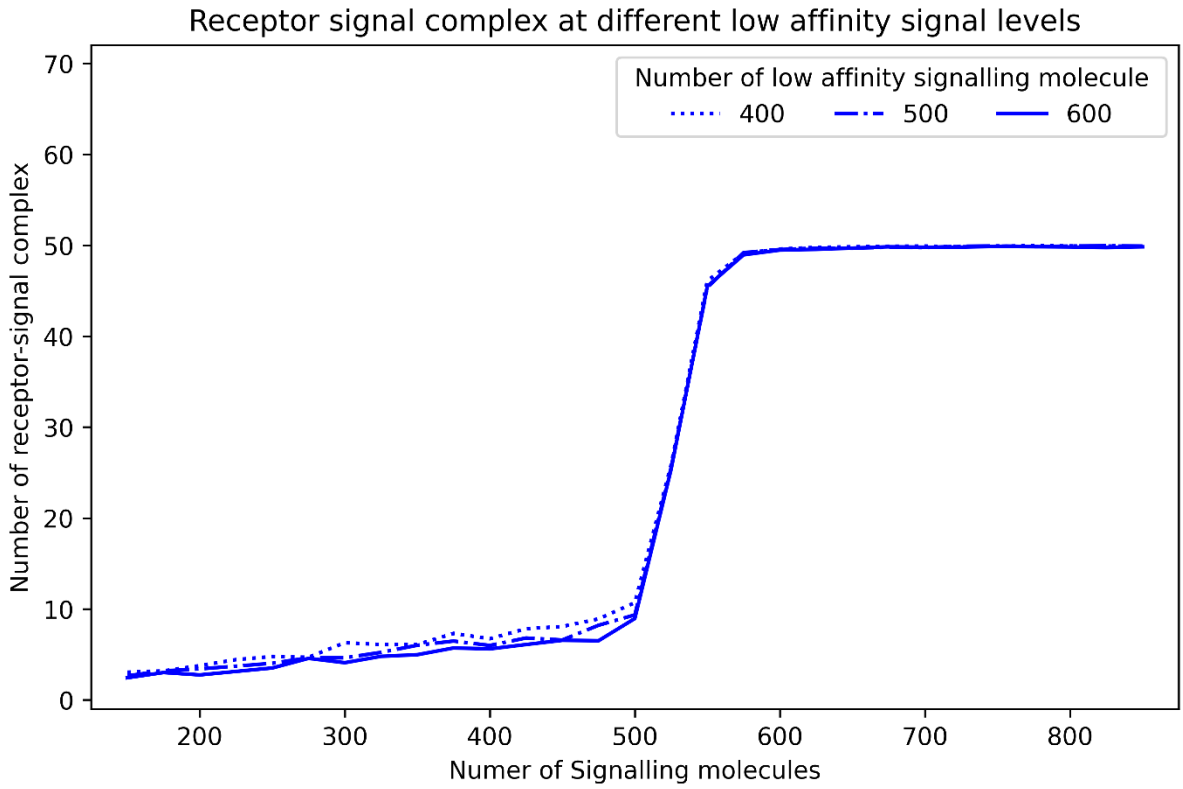

Figure A8: Dependence of receptor activation in varying levels of decoy signaling molecules. The parameters used were same as that in Figure 5.